Finite Element Analysis Predicts Large Optic Nerve Head Strains During Horizontal Eye Movements

Xiaofei Wang,[1] Helmut Rumpel,[2] Winston Eng Hoe Lim,[2] Mani Baskaran,[3,4] Shamira A. Perera,[3,4] Monisha E. Nongpiur,[3,4] Tin Aung,[3–5] Dan Milea,[3,4] and Michaël J. A. Girard[1,3]

[1]Ophthalmic Engineering & Innovation Laboratory, Department of Biomedical Engineering, Faculty of Engineering, National University of Singapore, Singapore
[2]Department of Diagnostic Radiology, Singapore General Hospital, Singapore
[3]Singapore Eye Research Institute, Singapore National Eye Centre, Singapore
[4]Duke-NUS, Singapore
[5]Department of Ophthalmology, Yong Loo Lin School of Medicine, National University of Singapore, Singapore

Correspondence: Michaël J.A. Girard, Ophthalmic Engineering & Innovation Laboratory, Department of Biomedical Engineering, National University of Singapore, Engineering Block 4, #04-8, 4 Engineering Drive 3, 117583 Singapore; mgirard@nus.edu.sg.

Submitted: December 19, 2015
Accepted: April 5, 2016

Citation: Wang X, Rumpel H, Lim WEH, et al. Finite element analysis predicts large optic nerve head strains during horizontal eye movements. *Invest Ophthalmol Vis Sci*. 2016;57:2452–2462. DOI:10.1167/iovs.15-18986

Purpose. We combined finite element (FE) analysis and dynamic magnetic resonance imaging (MRI) to estimate optic nerve head (ONH) strains during horizontal eye movements, and identified factors influencing such strains. We also compared ONH strains (prelamina, lamina cribrosa, and retrolamina strains) induced by eye movements to those induced by IOP.

Methods. The ocular globes and orbits of a healthy subject were visualized during horizontal eye movements (up to 13°), using dynamic MRI. A baseline FE model of one eye was reconstructed in the primary gaze position, including details from the orbital and ONH tissues. Finite element-derived ONH strains induced by eye movements were compared to those resulting from an IOP of 50 mm Hg. Finally, a FE sensitivity study was performed, in which we varied the stiffness of all ONH connective tissues, to understand their influence on ONH strains.

Results. Our models predicted that, during horizontal eye movements, the optic nerve pulled the ONH posteriorly. Optic nerve head strains following a lateral eye movement of 13° were large and higher than those resulting from an IOP of 50 mm Hg. These results held true even with variations in connective tissue stiffness. We also found that stiff sclerae reduced lamina cribrosa and prelamina strains during eye movements, but stiff optic nerve sheaths significantly increased those strains.

Conclusions. Our models predicted high ONH strains during eye movements, which were aggravated with stiffer optic nerve sheaths. Further studies are needed to explore links between ONH strains induced by eye movements and axonal loss in glaucoma.

Keywords: eye movements, glaucoma, lamina cribrosa, finite element analysis, magnetic resonance imaging

The "standard" biomechanical theory of glaucoma, which currently is gaining ground in ophthalmology, hypothesizes that IOP and cerebrospinal fluid pressure (CSFP) deform the optic nerve head (ONH) tissues, including the lamina cribrosa (LC), and that these deformations (directly or indirectly) drive retinal ganglion cell death.[1] However, IOP and CSFP are not the only loads that can yield ONH deformations. Extraocular muscles also have been suggested to increase ONH deformations during eye movements.[2] Eye movements commonly deform the optic nerve along its entire length,[3] and these deformations may be transmitted directly to the ONH. To date, to our knowledge no studies have yet evaluated the influence of eye movements on ONH biomechanics and glaucoma. Because the ONH is extremely sensitive to relatively small forces (IOP and CSFP), it would seem logical that larger forces (as those exerted by the extraocular muscles) also would influence ONH physiology and pathophysiology. Interestingly, recent studies have reported that eye movements are impaired in early and advanced glaucoma subjects.[4–7] Although the exact mechanism is unclear, a biomechanical link between eye movements and glaucoma may be possible.

The eye globe, rectus muscles, and optic nerve can be visualized in vivo during horizontal eye movements using magnetic resonance imaging (MRI).[8,9] Unfortunately, the current MRI resolution is too low to detect any deformations at the level of the ONH and LC. Therefore, computational techniques, such as the finite element (FE) method, needs to be combined with MRI to model the complex biomechanical environment of the ONH during eye movements and to estimate corresponding ONH strains.

The aim of this study was to use FE to estimate ONH strains during horizontal eye movements, to compare such models with MRI, and to compare such strain predictions with those resulting from a large IOP elevation. In addition, FE sensitivity studies were performed to assess and understand the factors responsible for causing high ONH strains during eye movements.

Methods

We combined FE with MRI to estimate ONH strains during eye movements. Finite element analysis is a tool used regularly by engineers to investigate complex, 3-dimensional (3D) structures, such as aircrafts and engines. It is being used increasingly in different areas of medical research.[10,11] Finite element

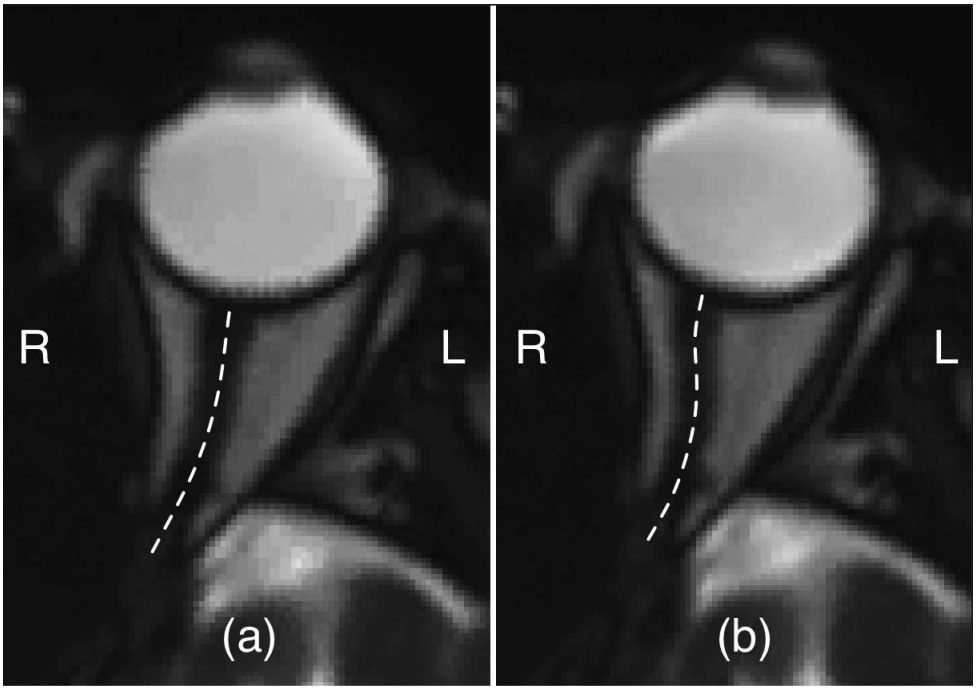

FIGURE 1. MRI images of a left eye (**a**) in primary position and (**b**) in lateral gaze to the left (13°), after a leftward movement. *Dashed lines* were added to illustrate the midlines of the optic nerve. Note that the curvature of the optic nerve exhibits distinguishable changes after a horizontal movement.

analysis can provide a quantitative characterization of the biomechanical environment of the ONH, given information about 3D eye geometry, tissue biomechanical properties, and boundary/loading conditions.

The images of a lateral gaze were first obtained using MRI and then a FE model was built to reproduce such a lateral gaze to estimate ONH strains induced by eye movements. Below is a detailed description of our MRI protocol and FE predictions.

Visualization of Eye Movements Using MRI

The optic nerve, orbital fat, rectus muscle, and eye globe movements of a single healthy subject were recorded in a 2-dimensional (2D) transverse plane using dynamic MRI. Continuous image acquisition of the subject's eyeballs was performed during internally generated, repeated pursuit eye movements using a 3T MRI scanner and a 32-channel head coil (Magnetom Skyra, Siemens Healthcare Sector, Erlangen, Germany). In this pursuit task, the supine subject was asked to follow a red moving target using an in-room viewing device (NordicNeuroLab AS, Bergen, Norway). The target was visible by both eyes and oscillating horizontally (approximately 13° of eccentricity) at a speed of 3°/s in a mesopic environment. True fast imaging with steady state precession (True FISP; Siemens, Munich, Germany) was performed at an acquisition time of 1 image per second with an in-plane resolution of 0.5 mm. Deformations of the optic nerve were observed as shown in Figure 1. The MRI protocol was approved by the SingHealth Centralized Institutional Review Board and adhered to the ethical principles outlined in the Declaration of Helsinki. Written informed consent was obtained from the healthy subject.

3D Digital Reconstruction of the Human Eye and Orbit

The geometry of the left eye (in primary gaze position; Fig. 1a) with its surrounding orbital tissues was digitally reconstructed from a 2D transverse MRI scan (Fig. 2). To generate a 3D model from the 2D scan, we assumed that the corneoscleral shell of the eye globe was a sphere (outer diameter, 24 mm; thickness, 1 mm) and that the coronal cross-section of the optic nerve was circular (diameter, 3.0–3.88 mm as obtained from the MRI image). Note that ONH tissue structures are not visible with MRI. Therefore, for our 3D reconstruction, we used a generic ONH geometry adapted from Sigal et al.[12] that incorporated the scleral flange (length, 0.4 mm; thickness, 0.45 mm), the LC (center thickness, 0.28 mm; anterior and posterior radii of 2.8 and 2.6 mm), and the prelaminar tissues (thickness, 0.2 mm). The ONH geometry was embedded within the spherical corneoscleral shell.

The optic nerve geometry consisted of three tissues: the nerve tissue, pia mater, and dura mater. The length of the optic nerve from the ONH to the orbital apex in the primary gaze position was 24.8 mm (measured manually from the MRI image). The thickness of the dura and that of the pia were set to averaged values reported in the literature and were 0.3[13] and 0.06[12] mm, respectively. Dural thickness was increased before merging with the peripapillary sclera at the level of the scleral flange (Fig. 2), as observed histologically.[14,15] The arachnoid mater was not included as it is extremely thin and close to the dura.[16] Extraocular muscle forces and deformations are not within the scope of this study; for simplicity, the extraocular muscles and the orbital fat were merged and simulated as a single entity. We will hereafter use OFM to refer to the orbital fat–muscle complex. The bony margins of the orbital walls were manually delineated from the MRI scan and incorporated to our geometry (Fig. 2). Note that the anterior part of the bony margin was not clearly visible in the MRI image; thus, we had to reconstruct it with information from other X-ray computed tomography images of healthy orbits (we used an anterior diameter of 35 mm).[17] Note also that the anterior portion of our 3D reconstructed eye geometry (anterior portion of the globe and fat) was simplified because we are not concerned with the stress/strain distributions in this area.

The reconstructed eye and orbit geometry was discretized into a hexahedron-dominant mesh with 55,020 8-node hexahedra and 64 6-node pentahedra (ABAQUS, Version 6.13; Dassault

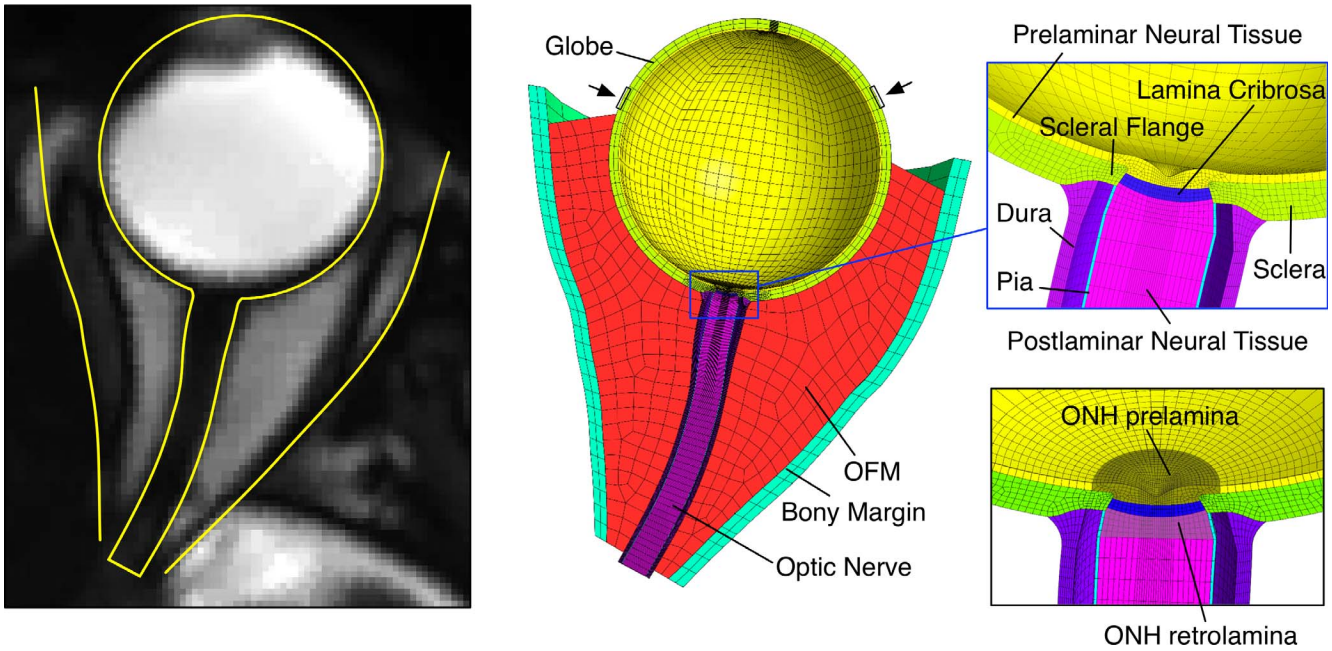

Figure 2. Reconstructed geometry and FE mesh of the eye model. The boundaries of the eye globe and optic nerve were manually delineated from the MRI scan; the bony margins of the orbit were manually delineated from the MRI scan, and with the help of other X-ray computed tomography images of healthy orbits.[17] Detailed ONH structures were included (sclera, LC, neural tissue, pia, and dura) using average measurements from the literature. *Top right*: enlarged view of the ONH region showing all ONH tissues considered in the FE models. *Bottom right*: illustrations of ONH prelamina and retrolamina. *Arrows* show muscle insertion regions.

Systèmes, Vélizy-Villacoublay Cedex, France; Fig. 2). The mesh density was numerically validated through a convergence test. Note that only half of the entire model was constructed as we assumed symmetry about the inferior-superior plane.

Assigning Stiffness Values to the Reconstructed Eye Tissues

To predict ONH tissue deformations with FE during eye movements, we must assign biomechanical properties (stiffness) to each reconstructed tissue. The biomechanical properties provide a link between stress (a measure of internal force) and strain (the gold-standard measure of deformation). Further measuring patient-specific biomechanical properties of eye tissues is not yet feasible. Thus, we used averaged biomechanical properties reported in the literature (Table 1).

The sclera and LC were modeled as fiber-reinforced composites.[18] The collagen fibers in the peripapillary sclera that surrounded the LC were organized into a ring (ring thickness, 0.6 mm).[19,20] Collagen fibers in other scleral regions

Table 1. Tissue Biomechanical Properties Used for the Baseline Model

Tissue	Constitutive Model*	Biomechanical Properties	References
Sclera	Mooney-Rivlin Von Mises distributed fibers	c1 = 0.805 MPa c3 = 0.0127 MPa c4 = 1102.25 θp: preferred fiber orientation†	Girard et al.[65]
Dura	Yeoh model	c1 = 0.1707 MPa c2 = 4.2109 MPa c3 = −4.9742 MPa	Porcine tissue experiment (this study)
LC	Mooney-Rivlin Von Mises distributed fibers	c1 = 0.05 MPa c3 = 0.0025 MPa c4 = 100 θp: preferred fiber orientation†	Zhang et al.[19]
Neural tissue	Isotropic elastic	Elastic modulus = 0.03 MPa Poisson's ratio = 0.49	Miller [66]
Pia	Yeoh model	c1 = 0.1707 MPa c2 = 4.2109 MPa c3 = −4.9742 MPa	Porcine tissue experiment (this study)
OFM	Isotropic elastic	Shear modulus = 900 Pa Poisson's ratio = 0.49	Schoemaker et al.[8]

* Constitutive models are mathematical equations derived from experiments and that describe the stress–strain (or force-deformation) relations for different tissues.

† Collagen fiber orientations were assigned to each element individually using a custom-written MATLAB code.

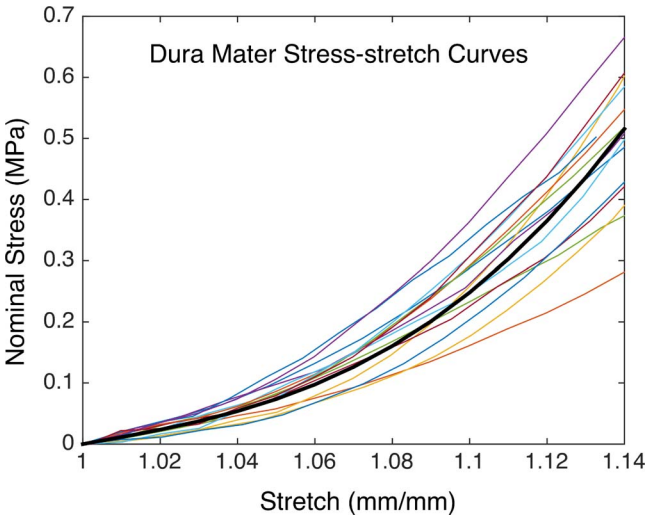

Figure 3. Uniaxial tension test results of porcine optic nerve dura maters. We used 15 longitudinal specimens from 15 optic nerves. The thickness of each sample was measured using a custom optical coherence tomography device (axial resolution, 4 μm).[64] After each sample (isolated length was approximately 15 mm) was mounted between the two grips of the uniaxial tensile tester, the length (grip-to-grip distance) and width of a sample were measured using a Vernier caliper (resolution, 0.01 mm). Samples were (mean ± SD) 7.62 ± 0.90 mm long, 6.23 ± 1.35 mm wide, and 0.19 ± 0.03 mm thick. The averaged stress–stretch response was fitted to a Yeoh model as indicated by the *bold line*. Nominal stress is the measured force divided by the original cross-sectional area of the sample.

were organized randomly (isotropy). The LC was modeled with radial collagen fibers (from the central vessel trunk to the scleral canal) but with low anisotropy as quantitatively assessed in humans, in our previous studies.[19,21] The neural tissue and orbital fat were considered isotropic and elastic and, thus, can be described with a single stiffness value (elastic modulus). Dural stiffness in the optic nerve region has not been reported in the literature. Therefore, we conducted uniaxial testing of porcine dural sheath (2 mm away from the ONH) along the longitudinal direction. Experiments were performed in compliance with the ARVO Statement for the Use of Animals in Ophthalmic and Vision Research. The averaged stress-stretch experimental data of 15 eyes were fitted using the Yeoh model[22] to extract corresponding biomechanical properties (Fig. 3). The stiffness of the pia mater (also unreported in the literature for the optic nerve region) was set to be the same as that of the dura mater, as both tissues contain abundant collagen fibers.[16] All soft tissues were considered incompressible (due to their high water content) and hyperelastic (allowing for large deformations). The orbital bone was modeled as a rigid body.

Friction Between Tissues and Other Boundary Conditions

A frictionless contact was assumed between the posterior globe tissues and orbital fat to simulate the small gap formed by Tenon's capsule.[23] The optic nerve and surrounding OFM were tied together at their interface based on previous studies[24] and our observation from dynamic MRI scans that these two tissues move together. The OFM was allowed to slide over the bony margin with a frictional coefficient of 0.5 (as measured for skeletal muscle and bone).[25] Of note, our preliminary studies demonstrated that ONH strains were insensitive to variations in this frictional coefficient. The optic nerve at the orbital apex was fixed to mimic its connection to the optic canal by fibrous adhesions.[26] The outer surface of the orbital bone also was fixed. Figure 4 illustrates all contact patterns between tissues and all boundary conditions in the model.

Loading Conditions – IOP and Eye Movements

An IOP of 15 mm Hg (applied to the inner limiting membrane),[27] a CSFP of 12.9 mm Hg (applied within the arachnoid space),[28] and an orbital tissue pressure of 4.4 mm Hg[29] (applied to the outer surface of globe and optic nerve) were used as loading conditions in the FE model (Fig. 4). These values represent

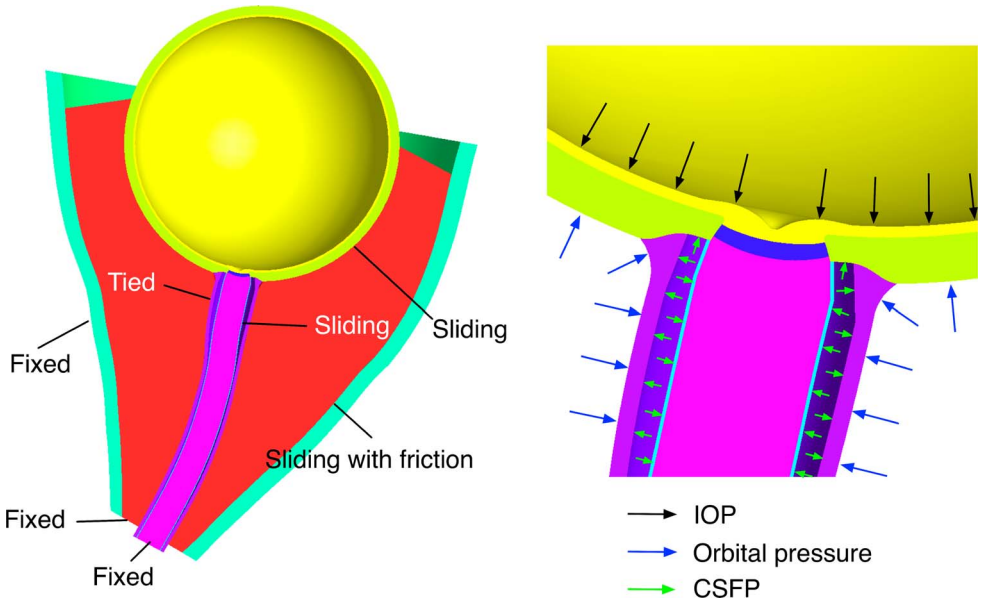

Figure 4. (*Left*) Boundary conditions (fixed optic nerve and OFM at the orbital apex; fixed outer bony margin surface) and surface boundary contact definitions (frictionless sliding contact between the posterior globe tissues and OFM, frictionless sliding contact between the pia and dura, tied contact between the optic nerve and OFM, sliding with friction contact between the OFM and bony margin). *Right*: Enlarged view of the ONH region illustrating the different pressure fields (IOP, CSFP, orbital pressure) applied to each model in the primary gaze position before eye rotation.

Investigative Ophthalmology & Visual Science

averaged normal pressures in the supine position, which are consistent with our MRI scanning body position.

To model a leftward eye movement from a primary gaze position, a rotation of 13° (as estimated from the MRI scans) about the superoinferior axis through the center of the eye was directly applied at the lateral rectus muscles' insertion regions (as nodal displacements representative of a 13° rotation; Fig. 2). The location of the insertions were estimated based on data from the literature.[30] The rotation value was extracted from the MRI scan. The eye movement duration in the FE model was 4 seconds to reproduce the in vivo conditions (pursuit task with MRI).

To estimate whether ONH strains induced by eye movements can be considered "large," we compared them to those resulting from a substantial increase in IOP. To this end, another loading scenario was considered, in which IOP was further increased from 15 to 50 mm Hg, but without eye movements.

Varying the Stiffness of Eye Tissues – FE Sensitivity Studies

The stiffness of eye tissues can vary considerably, even among healthy individuals.[31] In this study, we aimed to understand whether certain stiffness values could be responsible for high ONH strains during eye movements. To this end, we used a design of experiments (DOE) approach[32] to investigate how variations in the stiffness of collagenous tissues (sclera, LC, dura, and pia) could influence strains in sensitive ONH regions prone to axonal loss, such as the prelamina, LC, and retrolamina. The prelamina was defined as the portion of neural tissue directly above the LC and scleral flange. The retrolamina was defined as a portion of neural tissue (0.5 mm thick) posterior to the LC (Fig. 2). A four-factor two-level full factorial analysis was designed to allow examination of the effects of individual factors and all possible interactions of those factors. Here, the 4 factors broadly represent the stiffnesses of 4 connective tissues (LC, sclera, pia, and dura). However, because those tissues exhibit nonlinear properties, the stiffness of a given tissue cannot be represented as a single number. For simplicity, we, therefore, considered that a single factor represented all material coefficients for a given tissue (e.g., coefficients c1, c2, c3 for the dura). A high and low level were assigned for each factor. To rank the impact of factors, a reasonable physiologic range of these factors should be used. Unfortunately, tissue stiffness data are scarce in the literature and, even when reported, the values can vary considerably across studies. Therefore, for a given tissue, the low and high levels were set by varying all material coefficients (e.g., coefficients c1, c2, c3 for the dura) simultaneously by 20% around their baseline values to obtain their trends of effects (see Supplementary Material A). A total of 16 FE simulations (see Supplementary Material B), reflecting all possible combinations of high and low levels for each factor, were performed.

FE Processing to Predict Strain in the ONH

All FE models were solved using FEBio, a nonlinear FE solver designed for biomechanical studies.[33] For each model, we reported the first principal strain (mean and peak) in the prelamina, LC, and retrolamina following an increase in IOP (15 and 50 mm Hg) and following eye movements. Note that the first principal strain (unitless) is a standard engineering measure that represents the maximum local deformation exhibited by tissues.

The results of the FE sensitivity study were analyzed using MATLAB (Version 2014b; Mathworks, Inc., Natick, MA, USA). The mean strain levels induced by eye movement and those induced by IOP increase in all the models were compared using *t*-tests. The effects of factors were ranked based on their absolute values.

Comparing FE With MRI

To ensure that our baseline FE model was physiologically representative, we superimposed the FE-deformed boundary coordinates of the optic nerve and eye globe with the experimental MRI scan in the left gaze position.

Results

Qualitative Comparison – FE Versus MRI

We compared the corneoscleral shell and optic nerve outlines of our deformed FE geometry (baseline model) in the left gaze position with the MRI frame in its identical eye position. We found that our baseline model matched the MRI scan well (Figs. 5a, 5b).

ONH Strain Predictions – IOP Elevations and Eye Movements

During eye movements, we found that the optic nerve pulled the ONH posteriorly, which resulted in high strains within the ONH tissues. Specifically, for the baseline model, we reported strains (mean and peak) for the initial conditions (IOP = 15, CSFP = 12.9, orbital fat pressure = 4.4 mm Hg) in the prelamina, LC, and retrolamina (Fig. 2), as well as their increments due to either a leftward eye movement of 13° or an IOP elevation to 50 mm Hg (Table 2). We found that the strains generated within the prelamina, LC, and retrolamina following a leftward eye movement of 13° were higher (mean and peak) than those resulting from an IOP increase of 35 mm Hg (from 15–50 mm Hg). Strain distributions for all 3 cases are shown in Figure 6 for comparison. Note that we also simulated a rightward eye movement of the same angle. We found that the ONH strains were higher (17%) than those of a leftward eye movement (Supplementary Material C for the baseline model).

When all models were considered, we found that mean LC strains due to eye movements were higher than those resulting from an IOP of 50 mm Hg, and that peak LC strains were significantly higher (Table 3). For the prelamina and retrolamina, strains induced by eye movements all were significantly higher than those induced by an IOP of 50 mm Hg (Table 3).

Stiffness Factors Influencing ONH Strains During Eye Movements

We ranked the four main factors and their interactions using a linear regression model and the four most significant stiffness factors influencing ONH strains (in the prelamina, LC, and retrolamina) during eye movements were shown in Figure 7. Here, the horizontal bars represent the effects of individual stiffness factors or interactions of these factors. A longer bar indicates a more significant effect on ONH strains when varying stiffness from a low (–20% baseline) to a high (+20% baseline) value. Furthermore, in our context, a green bar is considered beneficial (ONH strain reduction) and a red bar detrimental (ONH strain increase).

We found that stiff sclerae and LCs reduced LC strains (mean and peak) during eye movements, but stiff dura and pia maters significantly increased those strains. These results held true for prelamina strains except that LC stiffness had almost no effects.

Interestingly, we also found that stiff dura maters shielded the retrolamina from exhibiting high strains, while stiff pia maters had the opposite effect. Stiffer sclerae increased the

Investigative Ophthalmology & Visual Science

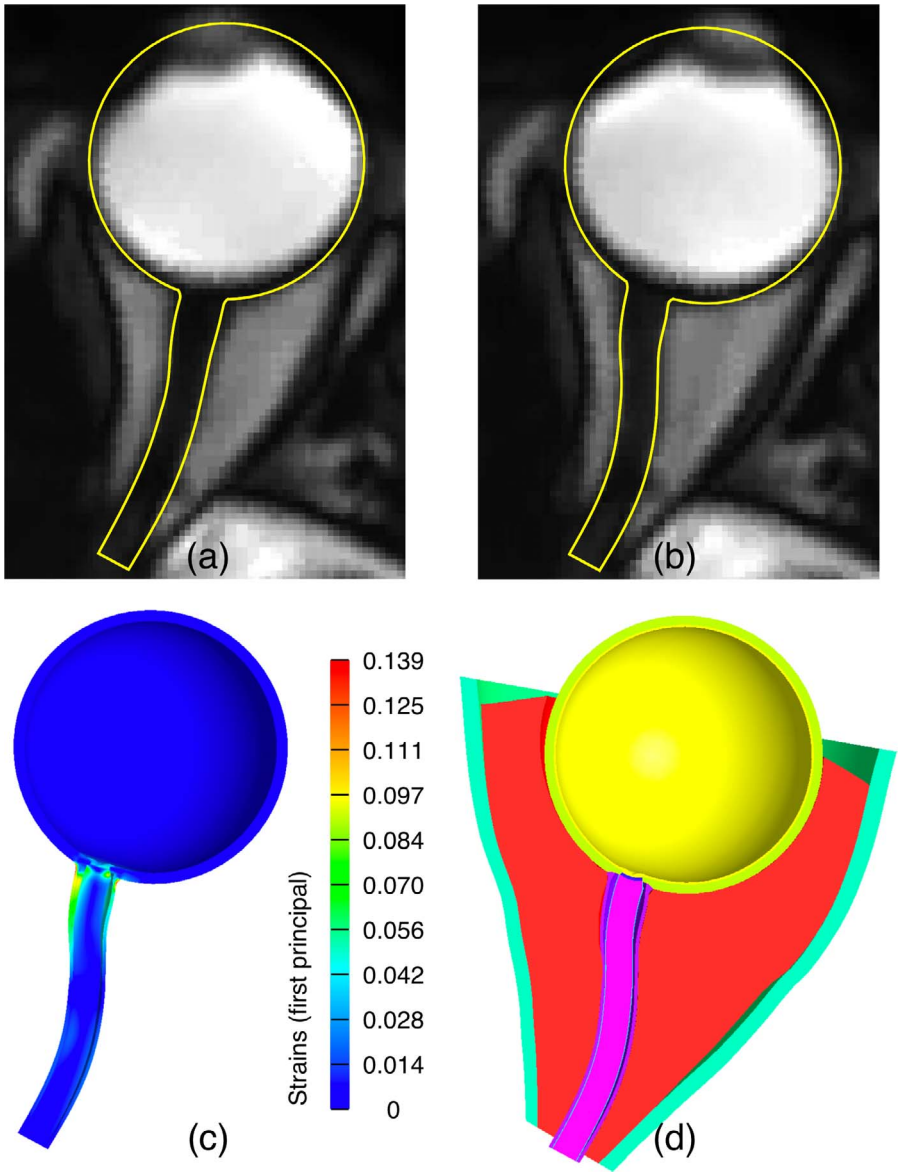

Figure 5. (**a**) Undeformed FE model of the eye globe and optic nerve (*yellow line*) superimposed on the MRI scan in primary gaze position. (**b**) Finite element predicted optic nerve boundary superimposed on the MRI scan in lateral gaze position. (**c**) Deformed globe and optic nerve with color-coded strains. (**d**) Complete FE model in the left gaze position.

mean strains in the retrolamina, while LC stiffness had little impact on all retrolamina strains.

For the prelamina and retrolamina, some interaction effects became significant but their magnitudes remained relatively small (Fig. 7).

Discussion

Our study combined dynamic MRI with FE analysis to understand how horizontal eye movements can influence the biomechanical environment of the ONH. Our models

Table 2. Mean and Peak First Principal Strains in the Prelamina, LC, and Retrolamina as Predicted by our Baseline Model (Unit, mm/mm)

	Prelamina		LC		Retrolamina	
	Mean Strain	Peak Strain	Mean Strain	Peak Strain	Mean Strain	Peak Strain
Initial conditions (IOP of 15, CSFP of 12.9, and orbital pressure of 4.4 Hg)	0.0015	0.0030	0.0026	0.0029	0.0015	0.0030
Leftward eye movement of 13°	0.0270	0.0495	0.0181	0.0351	0.0412	0.0708
IOP increase from 15 to 50 mm Hg in the primary position	0.0162	0.0443	0.0163	0.0277	0.0127	0.0191

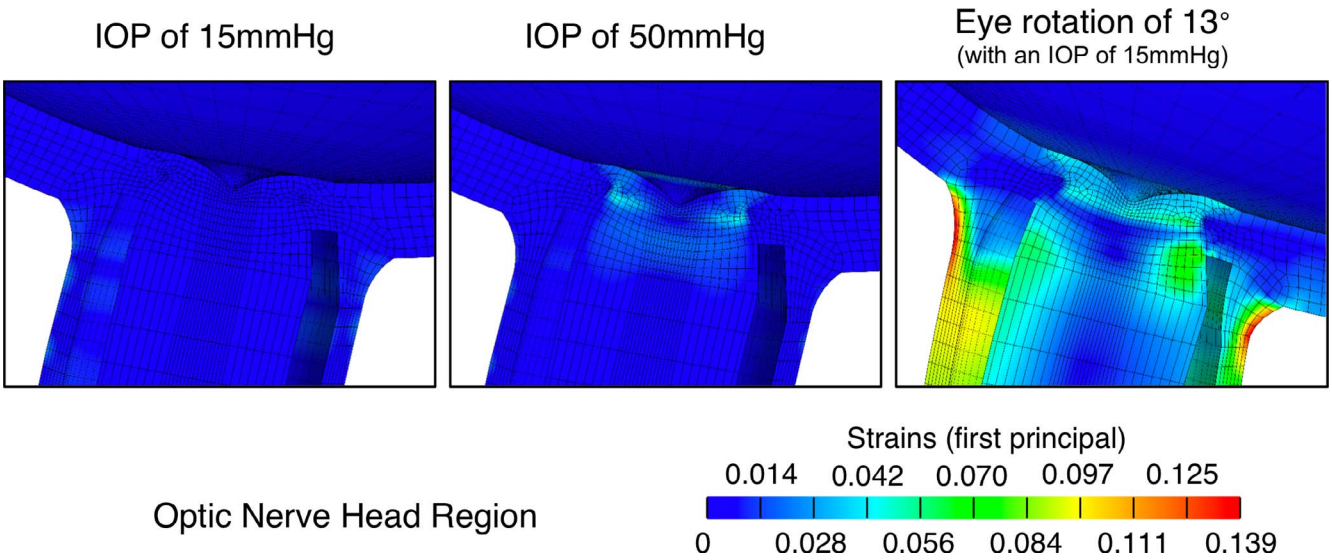

Figure 6. Optic nerve head deformations with color-coded strains for various loading scenarios. Note that, in addition to the loads indicated in the Figure, a CSFP of 12.9 mm Hg and an orbital tissue pressure of 4.4 mm Hg were applied on these three models as well.

predicted that, during eye movements, the optic nerve pulled the ONH posteriorly, which resulted in large strains within the ONH tissues (prelamina, LC, and retrolamina). These strains also were highly influenced by the stiffness of the surrounding connective tissue structures (peripapillary sclera, dura, pia, and LC).

FE Analysis Predicts High ONH Strain During Eye Movements

Our FE predictions showed that the mean and peak strains of the ONH tissues induced by an eye movement of 13° were larger than those induced by an IOP increase of 35 mm Hg (from a baseline of 15 mm Hg). It is important to emphasize that our predictions remained consistent even after variations in connective tissue stiffness within our FE models. Given that human eyes can rotate up to a maximum of approximately ±50° in daily activities,[34] even larger ONH deformations following eye movements should be expected.

Stiff Optic Nerve Sheaths Increase Prelamina and LC Strains During Eye Movements

Our FE sensitivity study suggested that the stiffer the optic nerve sheath tissues (dura and pia maters), the higher the prelamina and LC strains during eye movements. This finding is relatively intuitive, as a stiffer optic nerve sheath will tend to restrict the eye movement by exerting a larger pulling force on the globe.

The fact that the optic nerve can exert a significant pulling force on the globe and distort the intraocular tissues has been briefly mentioned in the literature. For instance, it has been speculated that the posterior pulling of the optic nerve sheaths on the peripapillary sclera was responsible for the presence of peripapillary intrachoroidal cavitations in highly myopic eyes due to the dehiscence between the sclera and choroid.[35,36] Other recent studies have demonstrated a phenomenon of optic nerve straightening during eye movements using MRI. In highly myopic patients, such a straightening resulted in a pulling force so strong that it retracted the eyeball within its own orbit by as much as approximately 7 mm (Demer JL, *IOVS* 2015;56:ARVO E-Abstract 1329).

It is interesting to note, that in the primary gaze position, the optic nerve is "slack," meaning that the intraorbital portion of the optic nerve is longer than the distance between the apex of the orbit and ONH.[37] In other words, the optic nerve will most often be curved (rather than straight) in its primary gaze position as observed in our MRI scans (Fig. 1a) and as taken into account in our FE models. It is highly plausible that the amount of optic nerve slack could vary across healthy individuals and across pathologies. To the best of our knowledge, this has not been reported. If it were the case, a smaller amount of slack in some individuals would intuitively result in larger ONH deformations during eye movements due to a rapid straightening effect, but this remains to be demonstrated. It is worth noting that stretching of the optic nerve is a rare, albeit possible, complication of proptosis in thyroid eye disease. The continuous optic nerve stretching may

Table 3. Mean and Peak First Principal Strains (Mean ± SD of 16 models) in the Prelamina, LC, and Retrolamina for All the Sensitivity Study Models (Unit, mm/mm)

	Prelamina		LC		Retrolamina	
	Mean Strain	Peak Strain	Mean Strain	Peak Strain	Mean Strain	Peak Strain
Leftward eye movement of 13°	0.027 ± 0.002	0.049 ± 0.004	0.018 ± 0.002	0.035 ± 0.003	0.041 ± 0.003	0.071 ± 0.004
IOP increase from 15 to 50 mm Hg in the primary position	0.017 ± 0.002	0.045 ± 0.006	0.017 ± 0.002	0.028 ± 0.004	0.013 ± 0.002	0.019 ± 0.002
P value	<0.0001*	0.02*	0.08	<0.0001*	<0.0001*	<0.0001*

* Indicates statistically significant differences. $P < 0.05$ was considered statistically significant.

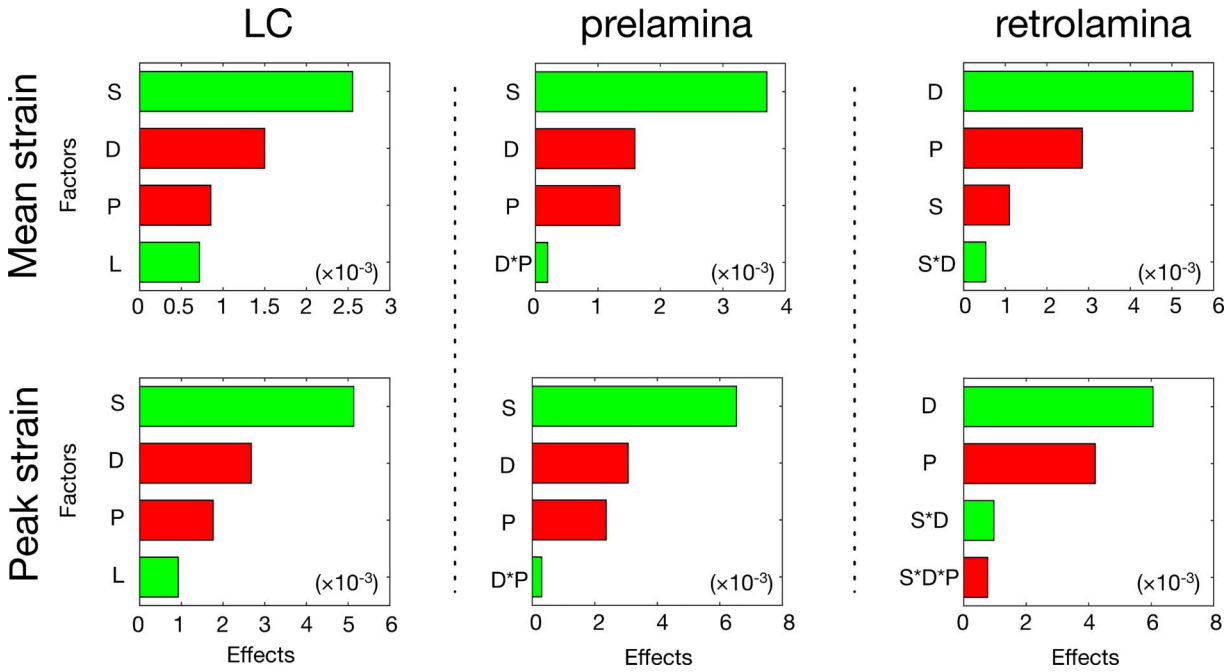

Figure 7. Ranking of the effects of connective tissue stiffness factors (only the four most significant factors were shown) on the mean and peak ONH strains (prelamina, LC, and retrolamina). *Green bars* indicate positive effects (ONH strain reduction) and *red bars* negative effects (ONH strain increase). S, sclera; D, dura; L, LC; P, Pia.

cause axonal death and optic neuropathy,[38] but little is known about the consequences of lateral eye movements on the optic nerve axons in this setting.

Stiff Dura Maters Reduce Retrolamina Strains During Eye Movements

Interestingly, we found that the stiffer the dura, the smaller the strains (mean and peak) in the retrolamina portion of the nerve (defined immediately below the LC). This result may appear counterintuitive, and directly contradicts the strain behaviors observed in the prelamina and LC. However, while a stiff dura may exert a pulling action on the ONH, it also will shield the optic nerve from exhibiting large amounts of bending. Thus, low optic nerve bending near the ONH could explain the low retrolamina strains.

Stiff Sclerae Reduce Prelamina and LC Strains During Eye Movements

Our sensitivity studies showed that the stiffness of the sclera was the most important factor to reduce prelamina and LC strains during eye movements. This finding is intuitive and consistent with other studies that have investigated the effects of factors on IOP-induced prelamina and LC strains.[19,39] While the optic nerve sheaths can exert a pulling action on the ONH during eye movements, it is logical that such effects would be limited by a stiff sclera, as the dura and pia maters directly anchor to the peripapillary sclera. Since the LC and prelamina are considerably weaker than the peripapillary sclera,[39] any deformations from the sclera due to eye movements would be directly transmitted to those tissues.

Eye Movements and Glaucoma: A Biomechanical Link?

If large ONH strains are observed with eye movements, one could suspect a biomechanical link with glaucoma. We know that the main site of retinal ganglion cell damage in glaucoma is the LC.[40,41] Furthermore, circumstantial evidence now suggests that LC strains may drive ganglion cell death (directly or indirectly).[1,42–44] While previous studies have estimated LC strains induced by increased IOP[1,45] or increased trans-LC pressure differences,[28,46] none has yet considered eye movements as a significant source of deformations.

Incidentally, several studies have reported that eye movements were abnormal in glaucoma subjects, which was reflected in their daily activities, such as driving[47] and reading.[5,7] Glaucoma subjects had a lower average rate[48,49] and a longer latency[6,50] of saccades compared to normal controls. Most likely, abnormal eye movements could be part of an adaptive strategy to compensate for vision loss, but nothing yet excludes that abnormal eye movements could have a causative role in the development and progression of glaucoma.

Note that ONH strains induced by eye movements are transient while IOP-induced strains are sustained and chronic. By itself, this fact could discredit the hypothesis that eye movements could have a considerable role in glaucoma. However, transient strains could have long-term impacts on the ONH tissues because our eyes exhibit frequent movements in daily activities (approximately 170,000 saccades per day[51]) and even during sleep (e.g., rapid eye movement sleep[52]). Furthermore, if eye movements have the ability to distort the intraocular tissues, they could possibly alter IOP in susceptible individuals, and this has yet to be explored. A better understanding of the differences in eye movement patterns and ONH biomechanics between normal and glaucoma subjects currently is required.

Limitations

In this study, several limitations warrant further discussion. First, the ONH strain values we reported were predicted by FE analysis and were not directly measured in vivo, as no such measurements can yet be obtained. This is consistent with the

large majority of studies that have been performed on ONH biomechanics.[53,54] Yet, to increase the confidence of our estimates, we have: (1) compared the global shape of our model with MRI, and (2) performed a sensitivity study proving that our results held true even with variations in connective tissue stiffness. Note that due to the low resolution of the MRI images, we can only compare the global shape of the optic nerve qualitatively (MRI versus FE) to increase the confidence of our FE model. In future studies, quantitative measures, such as strains, should be used to validate the model as they become available.

Second, we reconstructed the eye and orbit geometries from a single eye only, and the ONH from average measurements in the literature (as MRI could not resolve the ONH structures). In our sensitivity studies, we only investigated the variations in connective tissue stiffness on ONH strains while maintaining all morphologic factors the same. However, ONH and optic nerve geometries also vary across individuals and, thus, might have significant influences on the ONH strains. Future studies should include morphologic variations to account for individual differences. This also may have important implications for high myopia (thin sclera and regional variations in LC).[55,56]

Third, to rank the connective tissue stiffness factors, we varied the stiffness parameters by 20% of their baseline values, as proper physiologic ranges for each parameter are not available in the literature. As a result, stiffness variations from stiffer tissues were higher, which could have inflated the influence of the sclera in our ranking of effects. Note that this is not affecting any of the trends that we reported (e.g., stiff dura = more strain). Note also that previous sensitivity studies on ONH biomechanics determined the ranges of tissue stiffness by using scaling factors, which is similar to our assumption.[39,57]

Fourth, in this study, we experimentally measured the biomechanical properties of porcine optic nerve dura and used such properties for the dura and pia in all FE models. It is possible that the pia and dura exhibit different biomechanical properties, and that such properties also would be different across species. Studies that measured the biomechanical properties of human dura and pia have been performed but only for cranial and spinal tissues.[58,59] Although optic nerve dura and pia are considered extensions of cranial meninges, it has been reported that collagen fiber structures of optic nerve sheaths are very different from those of cranial meninges, suggesting strong differences in biomechanical properties.[60] Future experimental studies should be done to measure the biomechanical properties of human optic dura and pia mater, which will help us refine the proposed FE models. Additionally, in our experiments, the length-to-width ratios for all specimens were low (on average 1.28), which may have resulted in nonhomogeneous stress/strain fields within each specimen due to constraints of the specimens at the two grips (boundary effects). However, as the stretch was moderate (stretch ratio less than 20%), there was no observable "necking" of the specimens and a relative homogenous stress/strain field could be achieved. Therefore, we assumed a homogenous stress/strain field in the fitting of the constitutive model and potential boundary effects were not considered. In future studies, "dog-bone" shaped specimens with a very large length-to-width ratio could be used to minimize the boundary effects.

Fifth, viscoelastic behaviors were not included in this preliminary study because: (1) the corresponding properties are not available in the literature and (2) the eye rotated at a relatively low speed in the simulation (4 seconds for a rotation of 13°). Including viscoelastic effects in future studies will help us understand how the ONH would respond to different eye movement speeds.

Sixth, we assumed that the eye and optic nerve were symmetric about a 2D plane to generate a 3D model from a 2D MRI slice. This assumption was made based on the facts that the location of the 2D MRI slice was carefully determined during acquisition so that it divided the optic nerve and eye into halves, and the optic nerve lay within a 2D axial plane. This assumption may not be valid for patients with a "tortuous" optic nerve. In future studies, 3D MRI with high spatial resolution is required to take into account all possible anatomical variations across patients.

Seventh, we allowed the OFM to slide over the bony margin and did not consider a tied interface instead. We made this assumption based on the fact that considerable sliding of the OFM tissues near the bony margin can be observed with MRI during extraocular muscle contractions. Interestingly, we found that LC strains were 18% higher in the hypothetical scenario in which the OFM was tied to the bony margin (see Supplementary Material C). In future studies, detailed anatomical structures of the OFM and orbital wall should be included and appropriate connections between tissues should be assigned.

Eighth, our models may not have considered the right amount of optic nerve "slack" that is present in vivo. While the Yeoh model[22] was able to capture the uncrimping of the collagen fibers, it may have underestimated the original amount of crimp present in the tissues in vivo (and, thus, the optic nerve "slack"). On the other hand, prestretch also may exist in the optic nerve sheaths in vivo in the primary gaze position, and this could potentially reduce the amount of "slack." Further work will be required to understand if the amount of slack incorporated in our FE models (based on ex vivo experiments) is representative of the in vivo status in the primary gaze position, as this may have influenced our ONH strains estimates.

Ninth, the collagen fibers in the peripapillary sclera were organized into a ring but other regions of the sclera were assumed to be isotropic. However, several studies have shown that the remaining posterior sclera also was anisotropic, although the degree of anisotropy was significantly lower than that in the peripapillary region.[19,20,61,62] A recent study by Coudrillier et al.[63] demonstrated that the anisotropy of the peripheral sclera could have effects (although very limited) on the IOP-induced LC strains; but it is unknown how such anisotropy could affect the ONH strains during eye movements. Future modeling studies could incorporate the collagen fiber distributions of the whole scleral shell to understand the associated impact on the ONH during eye movements.

Tenth, the optic nerve at the orbital apex was fixed to mimic its connection to the optic canal by collagenous fibrous adhesions.[26] However, it still is unclear how strong this connection is. To look into the effects of this constraint, we ran another simulation in which this constraint was relaxed by fixing the optic nerve at the optic chiasm (to which it is attached) and allowing the optic nerve to slide over the optic canal (see Supplementary Material C). Our simulation results showed that there was a 7% reduction in LC strains, which was considered small. Further, all our conclusion remained valid even when considering the proposed relaxed constrained. In future studies, more accurate constraints of the optic nerve must be considered to increase the predictability of our models.

Conclusions

Our study combined FE with MRI to estimate ONH strains during eye movements. Our models predicted high ONH strains during eye movements, which increased with stiffer

optic nerve sheaths. Further studies are needed to explore a possible link between ONH strains induced by eye movements and axonal loss in glaucoma.

Acknowledgments

Supported by the Singapore Eye Research Institute Pilot Grant (R1228/34/2015), the Ministry of Education, Academic Research Funds, Tier 1 (R-397-000-181-112; R-397-000-140-133), and an NUS Young Investigator Award (NUSYIA_FY13_P03, R-397-000-174-133; MJAG).

Disclosure: **X. Wang**, None; **H. Rumpel**, None; **W.E.H. Lim**, None; **M. Baskaran**, None; **S.A. Perera**, None; **M.E. Nongpiur**, None; **T. Aung**, None; **D. Milea**, None; **M.J.A. Girard**, None

References

1. Burgoyne CF, Downs JC, Bellezza AJ, Suh JKF, Hart RT. The optic nerve head as a biomechanical structure: a new paradigm for understanding the role of IOP-related stress and strain in the pathophysiology of glaucomatous optic nerve head damage. *Prog Retin Eye Res*. 2005;24:39–73.
2. Greene PR. Mechanical considerations in myopia - relative effects of accommodation, convergence, intraocular-pressure, and the extra-ocular muscles. *Am J Optom Phys Opt*. 1980;57:902–914.
3. Botha CP, De Graaf T, Schutte S, et al. MRI-based visualisation of orbital fat deformation during eye motion. *Math Visual*. 2008;221–233.
4. Glen FC, Smith ND, Crabb DP. Saccadic eye movements and face recognition performance in patients with central glaucomatous visual field defects. *Vision Res*. 2013;82:42–51.
5. Burton R, Smith ND, Crabb DP. Eye movements and reading in glaucoma: observations on patients with advanced visual field loss. *Graef Arch Clin Exp*. 2014;252:1621–1630.
6. Lamirel C, Milea D, Cochereau I, Duong MH, Lorenceau J. Impaired saccadic eye movement in primary open-angle glaucoma. *J Glaucoma*. 2014;23:23–32.
7. Nguyen AM, van Landingham SW, Massof RW, Rubin GS, Ramulu PY. Reading ability and reading engagement in older adults with glaucoma. *Invest Ophthalmol Vis Sci*. 2014;55:5284–5290.
8. Schoemaker I, Hoefnagel PPW, Mastenbroek TJ, et al. Elasticity, viscosity, and deformation of orbital fat. *Invest Ophthalmol Vis Sci*. 2006;47:4819–4826.
9. Piccirelli M, Luechinger R, Rutz AK, Boesiger P, Bergamin O. Extraocular muscle deformation assessed by motion-encoded MRI during eye movement in healthy subjects. *J Vis*. 2007;7(14):5.
10. Wang X, Neely AJ, McIlwaine GG, Lueck CJ. Multi-scale analysis of optic chiasmal compression by finite element modelling. *J Biomech*. 2014;47:2292–2299.
11. Girard MJA, Downs JC, Bottlang M, Burgoyne CF, Suh JKF. Peripapillary and posterior scleral mechanics-part II: experimental and inverse finite element characterization. *J Biomech Eng*. 2009;131:051012.
12. Sigal IA, Flanagan JG, Tertinegg I, Etbier CR. Finite element modeling of optic nerve head biomechanics. *Invest Ophthalmol Vis Sci*. 2004;45:4378–4387.
13. Hasenfratz G. Experimental studies on the display of the optic nerve. In: Ossoinig KC, ed. *Ophthalmic Echography*. The Netherlands: Springer; 1987:587–602.
14. Shen L, You QS, Xu X, et al. Scleral thickness in chinese eyes. *Invest Ophthalmol Vis Sci*. 2015;56:2720–2727.
15. Elkington AR, Inman CB, Steart PV, Weller RO. The structure of the lamina cribrosa of the human eye: an immunocytochemical and electron microscopical study. *Eye (Lond)*. 1990;4:42–57.
16. Anderson DR. Ultrastructure of meningeal sheaths. Normal human and monkey optic nerves. *Arch Ophthalmol-Chic*. 1969;82:659–674.
17. Hwang SH, Park CS, Cho JH, Kim SW, Kim BG, Kang JM. Anatomical analysis of intraorbital structures regarding sinus surgery using multiplanar reconstruction of computed tomography scans. *Clin Exp Otorhinolar*. 2013;6:23–29.
18. Girard MJA, Downs JC, Burgoyne CF, Suh JKF. Peripapillary and posterior scleral mechanics–Part I: development of an anisotropic hyperelastic constitutive model. *J Biomech Eng-T Asme*. 2009;131:051011.
19. Zhang L, Albon J, Jones H, et al. Collagen microstructural factors influencing optic nerve head biomechanics. *Invest Ophthalmol Vis Sci*. 2015;56:2031–2042.
20. Pijanka JK, Coudrillier B, Ziegler K, et al. Quantitative mapping of collagen fiber orientation in non-glaucoma and glaucoma posterior human sclerae. *Invest Ophthalmol Vis Sci*. 2012;53:5258–5270.
21. Jones HJ, Girard MJ, White N, et al. Quantitative analysis of three-dimensional fibrillar collagen microstructure within the normal, aged and glaucomatous human optic nerve head. *J R Soc Interface*. 2015;12:20150066.
22. O'Hagan JJ, Samani A. Measurement of the hyperelastic properties of 44 pathological ex vivo breast tissue samples. *Phys Med Biol*. 2009;54:2557–2569.
23. Kakizaki H, Takahashi Y, Nakano T, et al. Anatomy of Tenons capsule. *Clin Experiment Ophthalmol*. 2012;40:611–616.
24. Cirovic S, Bhola R, Hose D, et al. Computer modelling study of the mechanism of optic nerve injury in blunt trauma. *Br J Ophthalmol*. 2006;90:778–783.
25. Shacham S, Castel D, Gefen A. Measurements of the static friction coefficient between bone and muscle tissues. *J Biomech Eng-T Asme*. 2010;132:084502.
26. Hayreh SS. *Structure of the Optic Nerve. Ischemic Optic Neuropathie*. Berlin: Springer-Verlag; 2011:7–34.
27. Hollows FC, Graham PA. Intra-ocular pressure, glaucoma, and glaucoma suspects in a defined population. *Br J Ophthalmol*. 1966;50:570–586.
28. Ren RJ, Jonas JB, Tian GG, et al. Cerebrospinal fluid pressure in glaucoma: a prospective Study. *Ophthalmology*. 2010;117:259–266.
29. Riemann CD, Foster JA, Kosmorsky GS. Direct orbital manometry in patients with thyroid-associated orbitopathy. *Ophthalmology*. 1999;106:1296–1302.
30. Schutte S, van den Bedem SP, van Keulen F, van der Helm FC, Simonsz HJ. A finite-element analysis model of orbital biomechanics. *Vision Res*. 2006;46:1724–1731.
31. Chen K, Rowley AP, Weiland JD, Humayun MS. Elastic properties of human posterior eye. *J Biomed Mater Res A*. 2014;102:2001–2007.
32. Antony J. *Design of Experiments for Engineers and Scientists*, 2nd ed. Waltham, MA: Elsevier; 2014.
33. Maas SA, Ellis BJ, Ateshian GA, Weiss JA. Finite elementBio: finite elements for biomechanics. *J Biomech Eng*. 2012;134:011005.
34. Land MF. Eye movements and the control of actions in everyday life. *Prog Retin Eye Res*. 2006;25:296–324.
35. You QS, Peng XY, Chen CX, Xu L, Jonas JB. Peripapillary intrachoroidal cavitations. The Beijing eye study. *PLoS One*. 2013;8:e78743.
36. Dai Y, Jonas JB, Ling Z, Wang X, Sun X. Unilateral peripapillary intrachoroidal cavitation and optic disk rotation. *Retina*. 2015;35:655–659.
37. Juanes JA, Ruisoto P, Prats-Galino A, Framinan A, Riesco JM. Computed anatomical modelling of the optic pathway and oculomotor system using magnetic resonance imaging. *J Neurorad*. 2014;41:168–176.

Investigative Ophthalmology & Visual Science

38. Cascone P, Rinna C, Reale G, Calvani F, Iannetti G. Compression and stretching in graves orbitopathy: emergency orbital decompression techniques. *J Craniofac Surg*. 2012;23: 1430–1433.
39. Sigal IA, Flanagan JG, Ethier CR. Factors influencing optic nerve head biomechanics. *Invest Ophthalmol Vis Sci*. 2005; 46:4189–4199.
40. Bellezza AJ, Rintalan CJ, Thompson HW, Downs JC, Hart RT, Burgoyne CF. Deformation of the lamina cribrosa and anterior scleral canal wall in early experimental glaucoma. *Invest Ophthalmol Vis Sci*. 2003;44:623–637.
41. Quigley HA, Addicks EM, Green WR, Maumenee AE. Optic-nerve damage in human glaucoma. 2. The site of injury and susceptibility to damage. *Arch Ophthalmol-Chic*. 1981;99: 635–649.
42. Nickells RW, Howell GR, Soto I, John SWM. Under pressure: cellular and molecular responses during glaucoma, a common neurodegeneration with axonopathy. *Ann Rev Neurosci*. 2012;35:153–179.
43. Howell GR, Libby RT, Jakobs TC, et al. Axons of retinal ganglion cells are insulted in the optic nerve early in DBA/2J glaucoma. *J Cell Biol*. 2007;179:1523–1537.
44. Quigley HA, Hohman RM, Addicks EM, Massof RW, Green WR. Morphologic changes in the lamina cribrosa correlated with neural loss in open-angle glaucoma. *Am J Ophthalmol*. 1983; 95:673–691.
45. Girard MJA, Suh JKF, Bottlang M, Burgoyne CF, Downs JC. Biomechanical changes in the sclera of monkey eyes exposed to chronic IOP elevations. *Invest Ophthalmol Vis Sci*. 2011;52: 5656–5669.
46. Wang N, Xie X, Yang D, et al. Orbital cerebrospinal fluid space in glaucoma: the Beijing intracranial and intraocular pressure (iCOP) study. *Ophthalmology*. 2012;119:2065–2073.
47. Crabb DP, Smith ND, Rauscher FG, et al. Exploring eye movements in patients with glaucoma when viewing a driving scene. *PLoS One*. 2010;5:e9710.
48. Smith ND, Glen FC, Crabb DP. Eye movements during visual search in patients with glaucoma. *BMC Ophthalmol*. 2012;12: 45.
49. Smith ND, Crabb DP, Glen FC, Burton R, Garway-Heath DF. Eye movements in patients with glaucoma when viewing images of everyday scenes. *Seeing Perceiving*. 2012;25:471–492.
50. Kanjee R, Yücel Y, Steinbach M, González E, Gupta N. Delayed saccadic eye movements in glaucoma. *Eye and Brain*. 2012;4: 63–68.
51. Schiller PH, Tehovnik EJ. Neural mechanisms underlying target selection with saccadic eye movements. *Prog Brain Res*. 2005;149:157–171.
52. Hobson JA. REM sleep and dreaming: towards a theory of protoconsciousness. *Nat Rev Neurosci*. 2009;10:803–813.
53. Norman RE, Flanagan JG, Sigal IA, Rausch SMK, Tertinegg I, Ethier CR. Finite element modeling of the human sclera: influence on optic nerve head biomechanics and connections with glaucoma. *Exp Eye Res*. 2011;93:4–12.
54. Sigal IA, Flanagan JG, Tertinegg I, Ethier CR. Modeling individual-specific human optic nerve head biomechanics. Part I: IOP-induced deformations and influence of geometry. *Biomech Model Mechan*. 2009;8:85–98.
55. Jonas JB, Berenshtein E, Holbach L. Lamina cribrosa thickness and spatial relationships between intraocular space and cerebrospinal fluid space in highly myopic eyes. *Invest Ophthalmol Vis Sci*. 2004;45:2660–2665.
56. Rada JAS, Shelton S, Norton TT. The sclera and myopia. *Exp Eye Res*. 2006;82:185–200.
57. Sigal IA, Flanagan JG, Tertinegg I, Ethier CR. Modeling individual-specific human optic nerve head biomechanics. Part II: influence of material properties. *Biomech Model Mechanobiol*. 2009;8:99–109.
58. Vannoort R, Black MM, Martin TRP, Meanley SA. Study of the uniaxial mechanical-properties of human dura mater preserved in glycerol. *Biomaterials*. 1981;2:41–45.
59. Mazuchowski EL, Thibault LE. Biomechanical properties of the human spinal cord and pia mater. Summer Bioengineering Conference, Sonesta Beach Resort, Key Biscayne, FL, USA; 2003.
60. Raspanti M, Marchini M, Dellapasqua V, Strocchi R, Ruggeri A. Ultrastructure of the extracellular-matrix of bovine dura-mater, optic-nerve sheath and sclera. *J Anat*. 1992;181:181–187.
61. Danford FL, Yan DM, Dreier RA, Cahir TM, Girkin CA, Vande Geest JP. Differences in the region- and depth-dependent microstructural organization in normal versus glaucomatous human posterior sclerae. *Invest Ophthalmol Vis Sci*. 2013;54: 7922–7932.
62. Grytz R, Fazio MA, Libertiaux V, et al. Age- and race-related differences in human scleral material properties. *Invest Ophthalmol Vis Sci*. 2014;55:8163–8172.
63. Coudrillier B, Boote C, Quigley HA, Nguyen TD. Scleral anisotropy and its effects on the mechanical response of the optic nerve head. *Biomech Model Mechanobiol*. 2013;12: 941–963.
64. Liu X, Yu X, Tang H, et al. Spectrally encoded extended source optical coherence tomography. *Opt Lett*. 2014;39:6803–6806.
65. Girard MJA, Suh JKF, Bottlang M, Burgoyne CF, Downs JC. Scleral biomechanics in the aging monkey eye. *Invest Ophthalmol Vis Sci*. 2009;50:5226–5237.
66. Miller K. Constitutive model of brain tissue suitable for finite element analysis of surgical procedures. *J Biomech*. 1999;32: 531–537.

Investigative Ophthalmology & Visual Science